

TOTAL VARIATION ITERATIVE LINEAR EXPANSION OF THRESHOLDS WITH APPLICATIONS IN CT

Shahar Tsiper, Oren Solomon and Yonina C. Eldar

Technion — Israel Institute of Technology

ABSTRACT

The iterative linear expansion of threshold framework, or iLET, offers a new approach for solving image restoration problems under sparsity assumptions. Instead of estimating the reconstructed image directly, the iLET paradigm parametrizes the reconstruction process as a linear combination of elementary thresholding functions and optimizes over their coefficients. Here, we rely on the fast and accurate convergence of iLET, and propose an extension of this framework, under the assumption that the reconstructed object is approximately piece-wise constant. This assumption leads to a new total-variation framework of iLET. We demonstrate the applicability of our technique to bio-medical imaging problems, such as computerized tomography reconstruction. Our technique surpasses state-of-the-art reconstructions in terms of PSNR and SSIM, while offering an automatic way for tuning its regularization parameter.

Index Terms— Total Variation, Sparse Recovery, Convex Optimization, Computed Tomography

1. INTRODUCTION

Image restoration is a well known problem in the scientific literature. Recently, Pan and Blu [1] proposed a framework for image restoration under sparsity assumptions, known as the *iterative linear expansion of thresholds*, or iLET. The iLET approach consists of recovering a sparse signal $\mathbf{x} \in \mathbb{R}^N$ from noisy measurements $\mathbf{y} \in \mathbb{R}^M$, given by $\mathbf{y} = \mathbf{H}\mathbf{x} + \mathbf{n}$, where $\mathbf{n} \in \mathbb{R}^N$ denotes additive noise. Specifically, in the context of image denoising, they proposed a solution approximated by a linear combination of simple denoising steps on the input image [2, 3]. The weights were then optimized by minimizing an estimate of the MSE, termed SURE, or Stein’s unbiased risk estimate [4]. While the approximation basis can be chosen arbitrarily, the approximation quality is determined by the number of vector (or *threshold*) bases and their associated thresholding operations.

Pan and Blu then expanded these ideas to image restoration. Instead of optimizing the weights over an estimate of the MSE, a regularized majorization-minimization (MM) approach to sparse inverse problems, such as LASSO [5] was considered for optimizing the weights. The regularization parameter was updated iteratively using a simple update scheme. The final image was then synthesized from the optimal linear combination of LET vectors. The iterative LET scheme was shown to usually converge faster than state-of-the-art methods such as FISTA [6].

Here, we utilize the benefits of the iLET framework, i.e. fast and accurate convergence with computational efficiency, for the case of regularized isotropic TV minimization. By using a MM approach to

a TV regularized inverse problem and employing a fast TV denoising algorithm [7], we formulate a new TV-based iLET recovery scheme. We choose the iLET basis vectors to correspond to several simultaneous denoising steps with different scales of the regularization parameter. The outputs of these steps are combined with a simple iterative regularization parameter update rule, to allow a parameter-free reconstruction method, which does not require any prior knowledge of the noise variance. We provide several examples to the efficacy of our technique in medical imaging applications, specifically here, in computerized tomography (CT) reconstruction. Our method achieves superior reconstruction results compared to state-of-the-art methods, in terms of PSNR and SSIM, coupled with lower computational complexity and running time.

The paper is organized as follows. In the next section we summarize the iLET framework. Our main contribution, the adaption of the framework to TV regularization, is described in Section 3. Section 4 explains the auto-update process of the method’s regularization parameter. In Section 5 we describe and present the results of a simulation study, and conclude in Section 6.

2. ITERATIVE LINEAR EXPANSION OF THRESHOLDS

To understand the ideas behind TV-iLET, we follow the work of [1] and start with a brief overview of the iLET framework. Consider a linear measurement model $\mathbf{y} = \mathbf{H}\mathbf{x}$, where $\mathbf{H} \in \mathbb{R}^{M \times N}$. The operator \mathbf{H} can correspond to a convolution matrix with some blurring kernel, a CT scanning operator and more. The vector \mathbf{x} is assumed to be sparsely represented under a known basis, e.g. under the wavelet decomposition $\mathbf{W} \in \mathbb{R}^{N \times D}$, such that $\mathbf{x} = \mathbf{W}\mathbf{c}$ for some sparse coefficient vector \mathbf{c} , with $\|\mathbf{c}\|_0 \ll D$. A common way to estimate \mathbf{c} (and from it reconstruct \mathbf{x}) is to find the minimizer of the LASSO optimization problem

$$\min_{\mathbf{c}} J(\mathbf{c}) = \min_{\mathbf{c}} J_0(\mathbf{c}) + \lambda \|\mathbf{c}\|_1 \quad (1)$$

with $J_0(\mathbf{c}) = \|\mathbf{y} - \mathbf{H}\mathbf{W}\mathbf{c}\|_2^2$.

Problem (1) can be solved using many convex optimization solvers, such as (fast) iterative shrinkage/soft-thresholding (ISTA/FISTA) [6]. Another approach relies on the general MM framework [8]. An example of such an algorithm is *iterative reweighted least squares* (IRLS) [9]. Its core idea is to majorize the non-differentiable $\|\cdot\|_1$ term in (1) with a majorizing function. Specifically, the term $\|\mathbf{c}\|_1$ is written as

$$\|\mathbf{c}\|_1 = \mathbf{c}^T \mathbf{D}\mathbf{c},$$

with a diagonal matrix $\mathbf{D} \in \mathbb{R}^{D \times D}$ whose ii th element is $D_{ii} = \frac{1}{|c_i|}$ (or 0 if $|c_i|$ equals to zero). Fixing \mathbf{D} , the latter quadratic term is

Oren Solomon and Shahar Tsiper are equal contributors to this work. This project has received funding from the European Union’s Horizon 2020 research and innovation program under grant agreement No. 646804-ERC-COG-BNYQ and from the Ollendorf Foundation.

differentiable with respect to \mathbf{c} , and the minimizer of (1) is equivalently [10] the minimizer of

$$\mathbf{c}^{(n+1)} = \operatorname{argmin}_{\mathbf{c}} \|\mathbf{y} - \mathbf{H}\mathbf{W}\mathbf{c}\|_2^2 + \lambda \mathbf{c}^T \mathbf{D}^{(n)} \mathbf{c}, \quad (2)$$

where n is the iteration number. Each iteration of (2) admits a closed form solution

$$\mathbf{c}^{(n+1)} = \left((\mathbf{H}\mathbf{W})^T (\mathbf{H}\mathbf{W}) + \lambda \mathbf{D}^{(n)} \right)^{-1} (\mathbf{H}\mathbf{W})^T \mathbf{y},$$

where the diagonal of $\mathbf{D}^{(n)}$ is updated according to the previous iteration $\mathbf{c}^{(n)}$.

In the linear expansion of thresholds (LET) paradigm, the sparse coefficient vector \mathbf{c} is represented as a linear combination of *elementary basis vectors*, or processes, whose weights are further optimized. We denote the result of each such process on the measurement vector \mathbf{y} as $\mathbf{F}_k(\mathbf{y}) \in \mathbb{R}^D$, such that

$$\mathbf{c} = \sum_{k=1}^K a_k \mathbf{F}_k(\mathbf{y}) = \mathbf{F}\mathbf{a}. \quad (3)$$

The goal is to determine the optimal vector \mathbf{a} . Writing $\mathbf{F} = [\mathbf{F}_1(\mathbf{y}), \dots, \mathbf{F}_K(\mathbf{y})]$ and plugging (3) into (2) yields,

$$\mathbf{a}^{(n+1)} = \operatorname{argmin}_{\mathbf{a}} \|\mathbf{y} - \mathbf{H}\mathbf{W}\mathbf{F}\mathbf{a}\|_2^2 + \lambda (\mathbf{F}\mathbf{a})^T \mathbf{D}^{(n)} \mathbf{F}\mathbf{a}$$

with $D_{ii}^{(n)} = \left| 1 / [\mathbf{F}\mathbf{a}^{(n)}]_i \right|$ (or zero if the denominator tends to zero). The explicit expression for the optimal vector \mathbf{a} at each iteration is given by

$$\mathbf{a}^{(n+1)} = \left[\mathbf{F}^T \left(\mathbf{W}^T \mathbf{H}^T \mathbf{H} \mathbf{W} + \lambda \mathbf{D}^{(n)} \right) \mathbf{F} \right]^{-1} (\mathbf{H}\mathbf{W}\mathbf{F})^T \mathbf{y}.$$

Typically, K is chosen as a small number (between 4–7 in our tests), such that the latter matrix inversion is easily performed numerically. Thus, compared with IRLS performed directly on (1), the iterative LET technique is computationally more tractable, since the column dimension of \mathbf{F} is usually much smaller than the dimension of the recovered image.

To further refine the algorithm, it is possible to extend (3) such that the LET basis is constructed not only from the measurements \mathbf{y} , but also from the output of previous iterations, e.g., $\mathbf{F}_1 = \mathbf{c}^{(n)}$, $\mathbf{F}_2 = \mathbf{c}^{(n-1)}$, leading to the iterative LET.

Another possible type of iLET vectors are based on a “generalized gradient” of the non-differentiable function $J(1)$, defined as

$$\mathbf{F}_3 = \bar{\nabla}_{\tau} J(\mathbf{c}) = \frac{2}{\tau} \left[\mathbf{c} - \mathcal{T}_{\lambda\tau/2} \left(\mathbf{c} - \frac{\tau}{2} \nabla J_0(\mathbf{c}) \right) \right], \quad (4)$$

with the soft-thresholding operator

$$\mathcal{T}_{\alpha}(\mathbf{x}) = \max\{|\mathbf{x}| - \alpha, 0\} \cdot \operatorname{sign}(\mathbf{x}), \quad \alpha \geq 0. \quad (5)$$

In our TV approach we propose a generalized TV-based gradient and combine several such gradients to promote a piece-wise constant reconstruction without the need to hand-tune the value of λ .

3. TOTAL VARIATION ILET

Consider the TV minimization problem,

$$\min_{\mathbf{x}} \frac{1}{2} \|\mathbf{y} - \mathbf{H}\mathbf{x}\|_2^2 + \lambda \operatorname{TV}(\mathbf{x}), \quad (6)$$

with isotropic TV term $\operatorname{TV}(\mathbf{x}) = \sum_i \sqrt{(\Delta_i^h \mathbf{x})^2 + (\Delta_i^v \mathbf{x})^2}$, such that $\Delta_i^h = \mathbf{x}_i - \mathbf{x}_{r(i)}$ and $\Delta_i^v = \mathbf{x}_i - \mathbf{x}_{b(i)}$ represent horizontal

and vertical first-order derivatives with cyclic boundary conditions, respectively ($r(i)$ represents the pixel on the right of pixel i while $b(i)$ represents the pixel below pixel i).

We use the derivation of Oliveira *et al.* [11] of a quadratic majorizing function for the isotropic TV norm $\operatorname{TV}(\mathbf{x})$, given by the following function:

$$\operatorname{TV}(\mathbf{x}) \leq \mathbf{x}^T \mathbf{D}^T \mathbf{M}^{(n)} \mathbf{D} \mathbf{x} + C,$$

where $\mathbf{D} = [(\mathbf{D}^h)^T, (\mathbf{D}^v)^T]^T$ and $\mathbf{D}^h, \mathbf{D}^v$ represent the horizontal and vertical first-order differentiation matrices with cyclic boundary conditions; C is a constant and as such does not affect the minimization process, and will be omitted from here on. The matrix $\mathbf{M}^{(n)}$ is given by

$$\mathbf{M}^{(n)} = \begin{bmatrix} \mathbf{\Lambda}^{(n)} & \mathbf{0} \\ \mathbf{0} & \mathbf{\Lambda}^{(n)} \end{bmatrix}, \quad (7)$$

where $\mathbf{\Lambda}^{(n)}$ is a diagonal matrix whose i th element is given by (or is set to zero if the denominator tends to zero)

$$[\mathbf{\Lambda}^{(n)}]_{ii} = \left((\Delta_i^h \mathbf{x}^{(n)})^2 + (\Delta_i^v \mathbf{x}^{(n)})^2 \right)^{-1/2}. \quad (8)$$

Thus, (6) is replaced by

$$\min_{\mathbf{x}} \mathbf{x}^T \left(\frac{1}{2} \mathbf{H}^T \mathbf{H} + \lambda \mathbf{D}^T \mathbf{M}^{(n)} \mathbf{D} \right) \mathbf{x} - \mathbf{x}^T \mathbf{H}^T \mathbf{y}.$$

Assuming that \mathbf{x} is a linear combination of an iLET basis $\mathbf{x} = \mathbf{F}\mathbf{a}$, we can formulate the IRLS update rule,

$$\mathbf{a}^{(n+1)} = \left(\mathbf{F}^{(n)T} \left(\frac{1}{2} \mathbf{H}^T \mathbf{H} + \lambda \mathbf{D}^T \mathbf{M}^{(n)} \mathbf{D} \right) \mathbf{F}^{(n)} \right)^{-1} \mathbf{F}^{(n)T} \mathbf{H}^T \mathbf{y}. \quad (9)$$

Similarly to the previous section, we use a TV-based generalized gradient. Problem (6) can be viewed as a minimization of a more general decomposition model

$$\min_{\mathbf{x} \geq \mathbf{0}} f(\mathbf{x}) + \lambda g(\mathbf{x}), \quad (10)$$

where f is a smooth, convex function (such as $J_0(\mathbf{x})$) with a Lipschitz continuous gradient, and a possibly non-smooth but proper, closed and convex function g (for instance $\|\mathbf{x}\|_1$). We can iteratively solve (10) by finding *Moreau's proximal* (prox) mapping [12] of αg for some $\alpha \geq 0$, defined as

$$\operatorname{prox}_{\alpha g}(\mathbf{x}) = \operatorname{argmin}_{\mathbf{u} \in \mathbb{R}^n} \left\{ \alpha g(\mathbf{u}) + \frac{1}{2} \|\mathbf{u} - \mathbf{x}\|_2^2 \right\}. \quad (11)$$

For $g(\mathbf{x}) = \|\mathbf{x}\|_1$, $\operatorname{prox}_{\alpha g}(\mathbf{x})$ is given by the *soft-thresholding* operator (5). The generalized gradient step defined in (4) is based on the latter prox mapping.

In [7], the authors derived an iterative solution to the proximal mapping of the TV norm of an image $\operatorname{TV}(\mathbf{x})$, for both the isotropic and anisotropic cases. Considering the definition of the prox mapping (11), it is observable that the prox operator corresponds to a regularized denoising problem. Hence, we adopt the iterative TV-denoising procedure presented in the TV based FISTA formulation [7], denoted as algorithm $\operatorname{GP}_{\lambda}$, to formulate our generalized TV-gradient step. Intuitively, instead of performing a gradient step along the direction of the gradient of J_0 and then soft-thresholding, we apply a gradient step in the direction of the gradient of J_0 and then carry out a TV denoising step. This gradient is given by

$$\nabla J_{\lambda}(\mathbf{x}^{(n)})_{\operatorname{TV}} = \operatorname{GP}_{\lambda} \left\{ \mathbf{x}^{(n)} - \frac{1}{L_f} \mathbf{H}^T \left(\mathbf{H}\mathbf{x}^{(n)} - \mathbf{y} \right) \right\},$$

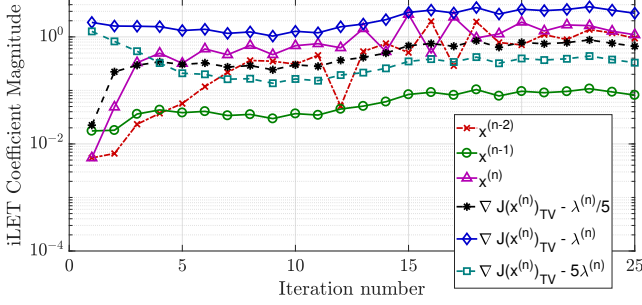


Fig. 1. The iLET coefficients evolution over the IRLS iterations. The different coefficients of the thresholds \mathbf{a}_k (3) shown in logarithmic scale, over the iterations as computed in (9), for the example in Fig. 2, left.

where L_f is the Lipschitz constant of the quadratic term of (6), readily given by $L_f = \|\mathbf{H}^T \mathbf{H}\|_2$.

In our experiments, we choose a total of 5 basis vectors for the TV-iLET method as follows:

$$\begin{aligned} \mathbf{F}_{1,2} &= \mathbf{x}^{\{(n-1), (n)\}} \\ \mathbf{F}_{3,4,5} &= \nabla J_{\left(\frac{1}{5}, 1, 5\right) \cdot \lambda} \left(\mathbf{x}^{(n)} \right)_{\text{TV}}. \end{aligned} \quad (12)$$

This configuration optimizes over the latest two iterations, as well as three different scales for TV regularization parameter λ , chosen empirically as $\{\frac{1}{5}, 1, 5\}$. To achieve superior results in terms of PSNR and SSIM, we use a combination of gradient steps with different scales for λ , along with a simple regularization update rule, as we present next. Figure 1 shows the values of the coefficients in each IRLS iteration, confirming that indeed each gradient step takes part in the formation of the final reconstructed object. The general description of the TV-iLET algorithm is summarized in Algorithm 1.

4. AUTOMATIC REGULARIZATION

The choice of the TV regularization parameter λ is obviously a non-trivial task, and in most modern applications this parameter is hand-tuned until achieving desirable results for private cases. Since the iLET-TV uses several basis vectors for composing the interim solution in every iteration, each with its own different scaling of λ , we observe that the quality of the final solution does not heavily depend on the initial choice of λ . Therefore, we propose to use the following update rule that automatically tunes a satisfactory value for λ . We first choose $\lambda^{(0)} = 0$ and perform a gradient step on the fidelity term, as shown in Algorithm 1. The regularization parameter is then updated in every iteration according to

$$\lambda^{(n)} = \frac{1}{2N} \left\| \mathbf{H}^T \mathbf{y} - \mathbf{H}^T \mathbf{H} \mathbf{x}^{(n)} \right\|_2,$$

where the factor $2N$ is used to normalize between the fidelity ℓ_2 norm and the TV norm, that operates on a total $2N$ (horizontal and vertical) spatial gradients of the image.

Note that asymptotically, for the true object \mathbf{x}_{opt} , λ converges to the noise variance. By updating the regularization constant to have the same magnitude as the fidelity residue, as well as combining gradient steps with different magnitudes for λ , in all of our tests we converge to accurate and relatively clean solutions. In Figs. 2 and 3 we compare to TV-based FISTA with the same update rule, and show

Algorithm 1 TV iLET

Require: L_f Lipschitz constant, measurements \mathbf{y}

Initialize $\mathbf{x}_0 = \mathbf{0}$

for $k = 1 : N_{\max}$ **do**

1: $\lambda^{(n)} \leftarrow \frac{1}{2N} \left\| \mathbf{H}^T \mathbf{y} - \mathbf{H}^T \mathbf{H} \mathbf{x}^{(n-1)} \right\|_2$

2: Update $\mathbf{F}^{(n)} \leftarrow [\mathbf{F}_1^{(n)}, \dots, \mathbf{F}_K^{(n)}]$ according to (12)

3: Construct $\mathbf{M}^{(n)}$ according to (7) and (8)

4: $\mathbf{a}^{(n)} \leftarrow [\mathbf{F}^{(n)T} (\frac{1}{2} \mathbf{H}^T \mathbf{H} + \lambda^{(n)} \mathbf{D}^T \mathbf{M}^{(n)} \mathbf{D}) \mathbf{F}^{(n)}]^{-1} \mathbf{F}^{(n)T} \mathbf{H}^T \mathbf{y}$

5: $\mathbf{x}^{(n)} = \mathbf{F}^{(n)} \mathbf{a}^{(n)}$

end for

return $\mathbf{x}^{(N_{\max})}$

that the TV-iLET scheme achieves better reconstruction. Thus, the combination of both the above update rule and the choice of different gradient steps is the key to achieve the highest reconstruction performance.

5. SETUP AND RESULTS

Medical images are usually considered as well approximated by piece-wise constant functions, as was shown in many works, among them [14–18], and specifically in CT. Motivated by testing our method on the problem of CT reconstruction, we chose to validate the iLET-TV algorithm on a simulated CT problem. The vast majority of reconstruction algorithms used today in CT scanners are based on filtered back projection (FBP) [19, 20] mainly due to its computational speed. However, various works have shown that there are great benefits [16, 17] employing modern iterative approaches for reconstructing tomographic measurements, reducing radiation and improving image quality. Since modern CT scanners are able to produce tens of thousands of measurements per each revolution of the X-ray tube, the measurements have an inherently large dimensionality. This fact is the main reason scanners today still rely on algorithms that were developed more than 30 years ago — applying a modern iterative solver for the dimensions involved in a scan is not feasible on available devices.

In our tests, we scan the Zubal [21] digitized brain phantom, and a thorax phantom rendered from a real patient scan. Both are with resolution of 256×256 ($N = 256$) and scanned with parallel-beam (PB) [19] tomographic simulator (AIR Tools v1.3 [22]). We acquire only 64 equally spaced angular projections of the phantom over a range of π radians, and contaminate the measurements with Gaussian noise with SNR of 28 dB.

The PB scan measurements are then transformed to the pseudo-polar (PP) [23–25] domain by employing the recent resampling algorithm for PP tomographic reconstruction (RAPToR) [26]. By working in the PP domain, we gain several advantages. The PP Radon transform (PPRT) (acting as \mathbf{H}) and the adjoint PPRT operator (\mathbf{H}^T) can be computed with a fast and accurate algorithm [24, 25] in $\mathcal{O}(N^2 \log N)$ complexity. In addition, the algebraic system that describes the PPRT has a significantly lower condition number than an equivalent PB system. Further advantages and discussions can be found in [26].

All the algorithms we test operate directly on the same PP measurements and the same system matrix. That way, the comparison between the algorithms is fair. We compare our method to the following algorithms: a PP based FBP followed by a TV denoiser, a FISTA+TV algorithm with a constant value for λ , a FISTA+TV algorithm updated with an iterative update step for the value of λ as discussed in Section 4 and to the sparse uniform resampling algorithm (SPURS) [13] followed by TV denoising.

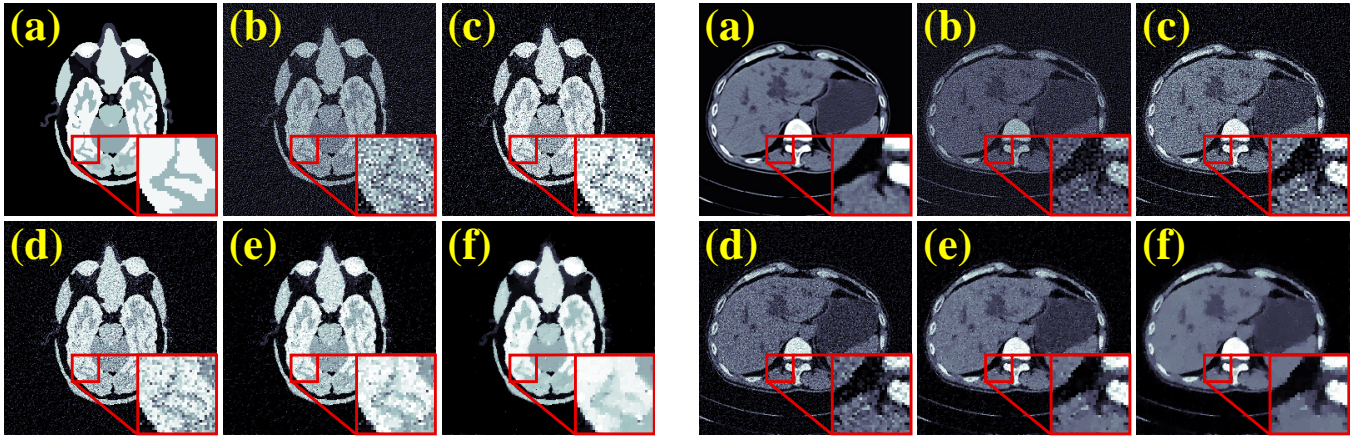


Fig. 2. Zubal and Thorax phantom reconstruction results. We reconstruct the Zubal (left batch) and the Thorax (right batch) phantoms from 64 PB projection angles, under SNR of 28 dB. The ground truth phantoms are shown in (a). The reconstructions for each phsantom include: (b) FBP, (c) FBP+TV, (d) FISTA+TV, (e) SPURS+TV [13] and (f) our TV-iLET method.

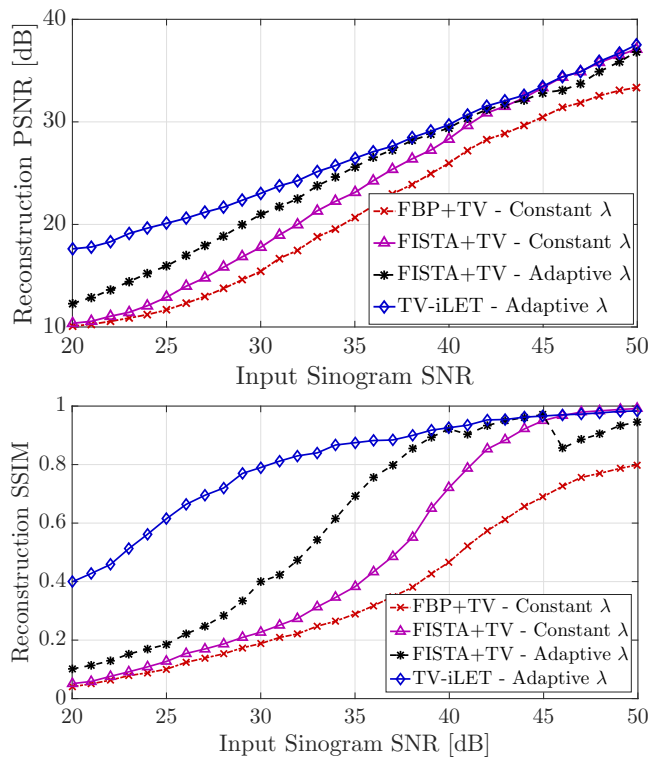


Fig. 3. TV-iLET Reconstruction graph comparisons. The horizontal axis depicts the input SNR (in dB) of the PB scan measurements. We measure the PSNR (top) and the SSIM (bottom) of the reconstructed output, compared with the ground-truth Zubal phantom, for several algorithms, as described in Section 5.

The results of our comparisons are shown as performance graphs, measuring the output peak-SNR (PSNR) and structural similarity index (SSIM) [27] vs. the input SNR of the measurements, and shown in Fig. 3. An example of the reconstructed phantoms for various algorithms is shown in Fig. 2. The TV-iLET algorithm achieves superior results throughout the input SNR range, while maintaining a low complexity.

6. CONCLUSIONS

In this work we presented an extension of the iLET paradigm to TV-based minimization. Our approach relies on majorizing the non-differentiable TV norm with a smooth quadratic term and minimizing over a set of basis vectors with a generalized TV-based gradient step. Our approach is also parameter free, and does not require empirical tuning of the regularization parameter. We demonstrate the superior performance of our technique on a medical imaging scenario, CT reconstruction, showing that the TV-iLET framework is applicable in this modality. Our method demonstrates low computational complexity and superior results over other state-of-the-art approaches, in terms of both PNSR and SSIM, as presented in Figs. 2 and 3.

References

- [1] H. Pan and T. Blu, "An iterative linear expansion of thresholds for l_1 -based image restoration," *IEEE Transactions on Image Processing*, vol. 22, no. 9, pp. 3715–3728, 2013.
- [2] F. Luisier, T. Blu, and M. Unser, "A new sure approach to image denoising: Interscale orthonormal wavelet thresholding," *IEEE Transactions on image processing*, vol. 16, no. 3, pp. 593–606, 2007.
- [3] T. Blu and F. Luisier, "The sure-let approach to image denoising," *IEEE Transactions on Image Processing*, vol. 16, no. 11, pp. 2778–2786, 2007.
- [4] Y. C. Eldar, "Generalized SURE for exponential families: Applications to regularization," *IEEE Transactions on Signal Processing*, vol. 57, no. 2, pp. 471–481, 2009.
- [5] Y. C. Eldar and G. Kutyniok, *Compressed sensing: theory and applications*. Cambridge University Press, 2012.
- [6] A. Beck and M. Teboulle, "A Fast Iterative Shrinkage-Thresholding Algorithm," *SIAM Journal on Imaging Sciences*, vol. 2, no. 1, pp. 183–202, 2009.
- [7] —, "Fast gradient-based algorithms for constrained total variation image denoising and deblurring problems," *IEEE Transactions on Image Processing*, vol. 18, no. 11, pp. 2419–2434, 2009.
- [8] K. Lange, *MM Optimization Algorithms*. SIAM, 2016.
- [9] I. Daubechies, R. DeVore, M. Fornasier, and C. S. Güntürk, "Iteratively reweighted least squares minimization for sparse recovery," *Communications on Pure and Applied Mathematics*, vol. 63, no. 1, pp. 1–38, 2010.
- [10] M. R. Osborne, *Finite algorithms in optimization and data analysis*. John Wiley & Sons, Inc., 1985.
- [11] J. P. Oliveira, J. M. Bioucas-Dias, and M. A. Figueiredo, "Adaptive total variation image deblurring: a majorization-minimization approach," *Signal Processing*, vol. 89, no. 9, pp. 1683–1693, 2009.
- [12] J.-J. Moreau, "Proximité et dualité dans un espace hilbertien," *Bulletin de la Société mathématique de France*, vol. 93, pp. 273–299, 1965.
- [13] A. Kiperwas, D. Rosenfeld, and Y. C. Eldar, "The SPURS Algorithm for Resampling an Irregularly Sampled Signal onto a Cartesian Grid," *IEEE transactions on medical imaging*, vol. X, no. X, pp. 1–16, 2016.
- [14] G. H. Chen, J. Tang, and S. Leng, "Prior image constrained compressed sensing (PICCS): a method to accurately reconstruct dynamic CT images from highly undersampled projection data sets," *Medical Physics*, vol. 35, no. 2, pp. 660–663, 2008.
- [15] E. Y. Sidky and X. Pan, "Image reconstruction in circular cone-beam computed tomography by constrained, total-variation minimization," *Physics in Medicine and Biology*, vol. 53, no. 17, pp. 4777–4807, 2008.
- [16] X. Pan, E. Y. Sidky, and M. Vannier, "Why do commercial CT scanners still employ traditional, filtered back-projection for image reconstruction?" *Inverse Problems*, vol. 25, no. 12, p. 123009, 2009.
- [17] J. S. Jorgensen and E. Y. Sidky, "How little data is enough? Phase-diagram analysis of sparsity-regularized X-ray CT," vol. 2014, no. 1, pp. 1–24, 2014.
- [18] C. Poon, "On the role of total variation in compressed sensing," *SIAM Journal on Imaging Sciences*, vol. 8, no. 1, pp. 682–720, 2015.
- [19] A. C. Kak and M. Slaney, *Principles of computerized tomographic imaging*. IEEE press, 1988.
- [20] J. Hsieh, *Computed Tomography: Principles, Design, Artifacts, and Recent Advances*. Bellingham: WA: SPIE, 2003.
- [21] I. G. Zubal, C. R. Harrell, E. O. Smith, Z. Rattner, G. Gindi, and P. B. Hoffer, "Computerized three-dimensional segmented human anatomy," *Medical Physics*, vol. 21, no. 2, pp. 299–302, 1994.
- [22] P. C. Hansen and M. Saxild-Hansen, "AIR tools - A MATLAB package of algebraic iterative reconstruction methods," *Journal of Computational and Applied Mathematics*, vol. 236, no. 8, pp. 2167–2178, 2012.
- [23] A. Averbuch, R. R. Coifman, D. L. Donoho, M. Israeli, and J. Waldén, "Fast slant stack: A notion of Radon transform for data in a Cartesian grid which is rapidly computable, algebraically exact, geometrically faithful and invertible," *SIAM Journal on Scientific Computing*, 2001.
- [24] A. Averbuch, R. Coifman, and D. Donoho, "A framework for discrete integral transformations I - the pseudopolar Fourier transform," *SIAM Journal on Scientific Computing*, vol. 30, no. 2, pp. 764–784, 2008.
- [25] A. Averbuch, R. Coifman, D. Donoho, Y. Shkolnisky, and I. Sedelnikov, "A framework for discrete integral transformations II - the 2D discrete Radon transform," *SIAM Journal on Scientific Computing*, vol. 30, no. 2, pp. 785–803, 2008.
- [26] S. Tsiper and Y. C. Eldar, "Raptor: A resampling algorithm for pseudo-polar based tomographic reconstruction," *arXiv preprint arXiv:1708.05163*, 2017.
- [27] Z. Wang, A. C. Bovik, H. R. Sheikh, and E. P. Simoncelli, "Image quality assessment: from error visibility to structural similarity," *IEEE transactions on image processing*, vol. 13, no. 4, pp. 600–612, 2004.